Generating and analyzing constrained dark energy equations of state and systematics functions

Johan Samsing[1] and Eric V. Linder[2,3]

[1]*Dark Cosmology Centre, Niels Bohr Institute, University of Copenhagen, Copenhagen, Denmark*
[2]*Berkeley Lab and University of California, Berkeley, California 94720, USA*
[3]*Institute for the Early Universe, Ewha Womans University, Seoul, Korea*

(Received 26 August 2009; published 23 February 2010)

Some functions entering cosmological analysis, such as the dark energy equation of state or systematic uncertainties, are unknown functions of redshift. To include them without assuming a particular form, we derive an efficient method for generating realizations of all possible functions subject to certain bounds or physical conditions, e.g. $w \in [-1, +1]$ as for quintessence. The method is optimal in the sense that it is both pure and complete in filling the allowed space of principal components. The technique is applied to propagation of systematic uncertainties in supernova population drift and dust corrections and calibration through to cosmology parameter estimation and bias in the magnitude-redshift Hubble diagram. We identify specific ranges of redshift and wavelength bands where the greatest improvements in supernova systematics due to population evolution and dust correction can be achieved.

DOI: 10.1103/PhysRevD.81.043533 PACS numbers: 98.80.−k, 95.36.+x

I. INTRODUCTION

The nature of the dark energy accelerating the cosmic expansion is a major mystery of modern physics. The effectively negative pressure giving rise to acceleration can be parametrized through the equation of state (EOS), or pressure to energy density, ratio of the dark energy. Observational quantities such as the distance-redshift relation, Hubble expansion rate, or matter density perturbation growth (assuming general relativity) can then be derived in terms of the EOS. However, little guidance exists from theory for the form of the EOS.

One of the standard approaches is to adopt a well-tested, nearly unbiased functional form for the EOS. For example, the EOS as a function of scale factor, $w(a) = w_0 + w_a(1 - a)$, where w_0, w_a are parameters to be fit, has been shown to be accurate at the 0.1% level in the observable distance for a wide array of dark energy models [1]. However, one may prefer to keep the EOS as free as possible. Values in bins of redshift, or some form of eigenmodes or principal components, do not impose assumptions on the form of $w(a)$ (see, e.g., [2–7]).

Physics does bound the possible behaviors, though, not allowing full freedom in the bin values or principal component coefficients. One example involves a minimally coupled, canonical scalar field, where for all redshifts the condition must hold that $w \in [-1, +1]$ for positive energy density. Principal components can be applied to many situations, such as the cosmic reionization fraction history or the fraction of a source population in a particular subclass, where values can only lie in [0, 1]. We generically call such unknown, redshift-dependent quantities ''state functions.'' Some approaches to such situations of ''freedom under constraint'' exist in the cosmology literature, e.g. [4,5,8–10], but here we concentrate on full and computationally efficient solutions.

Going further into the motivation, we consider three reasons for imposing bounds: physicality, efficiency, and prior information. Some physical bounds are absolute, such as an ionization fraction ranging between 0 and 1, while others are more relative, such as the dark energy equation of state ranging between -1 and $+1$ for a canonical, minimally coupled scalar field. In fact, there is a certain amount of framework dependence in any analysis—the matter density cannot be less than zero, but the effective matter density can appear less than zero when a universe with a cosmological constant is interpreted in terms of a pure matter universe: this is precisely how the acceleration of the Universe was discovered. So while physical bounds are generally valid, results pushing up against the bounds should sound a note of caution; one might then loosen the bounds to check for consistent results. But starting with overly loose or unmotivated bounds has the price of computational inefficiency; in the vast majority of cases one would not scan over a space where the ionization fraction ranged from -5 to $+5$, say. Finally, the bounds may arise from prior information such as having measured a calibration offset to be less than some value (as we apply in Sec. V). There is little point in examining the effect of larger variations than allowed by this prior information. These rationales for bounds on the state function then translate directly into the principal component space. We emphasize that only the amplitude, not the freedom in the functional form, is being limited.

When selecting physically valid principal component contributions, the two main issues are those of purity—every set of values gives a valid state function—and completeness—every possible valid state function is represented in the selection. In Sec. II we discuss possible methods for generating principal component realizations of the EOS (or any other) function and assess their purity and completeness, especially when only a subset of modes

is retained. We present a solution for the optimal—pure and complete—prescription in Sec. III, along with an efficient mathematical shortcut and visualization for implementing it. We then turn to state functions representing systematic uncertainties, whose evolution can cause incorrect cosmological conclusions. In Sec. IV we consider supernova population fractions as the constrained state function and investigate the biases this can impose on cosmological parameters, and how to best constrain these with redshift specific observations. We discuss dust extinction corrections and their interaction with filter calibration errors in Sec. V, and how to control these with wavelength specific measurements. The summary is presented in Sec. VI.

II. REALIZATIONS OF THE EQUATION OF STATE

We begin by phrasing the analysis in terms of the dark energy equation of state, although the results are generally applicable to any state function.

One possible goal for propagating an array of equation of state functions to observational constraints is to place as little prior constraint on the functions as possible, an admission of maximal ignorance in the hope that the observations impose form on chaos. A more restrained approach is to treat the form of *deviations* from the basic function as free, perhaps representing unknown systematic uncertainties, though bounded in amplitude in some way. The most direct approach then is to describe the deviations $w(z) - w_b(z)$ by some value in each small redshift bin, equivalent to expanding in a top-hat basis.

This can be transformed into any other orthogonal basis, and we can hope that a principal component analysis lets us compress the information in some way, such that a small, tractable number of modes gives a simplified, though still somewhat diverse, functional form. We can write

$$w(z) - w_b(z) = \sum_i \alpha_i e_i(z), \tag{1}$$

where we refer to $w(z) - w_b(z)$ as the state function, $e_i(z)$ as the modes or principal components, and α_i as the mode coefficients. Note that the state function is really the deviation from some baseline, and can represent the dark energy equation of state or the cosmic ionization fraction, supernova subclass population fraction, etc. In the top-hat basis, $e_i(z)$ would simply be 1 within the appropriate redshift bin and 0 outside, and α_i would simply be w_i, the value of the state function within the bin.

The state function may not be allowed to have arbitrary excursions, but can be constrained by physical or theoretical expectations to lie within some bounds. These bounds could be elementary, such as the ionization fraction must lie between 0 and 1, or more physical, such as the equation of state for a minimally coupled, canonical scalar field must possess $w(z) \in [-1, +1]$. We define the bounding function, or envelope, by

$$W_-(z) \le w(z) - w_b(z) \le W_+(z). \tag{2}$$

Given real data, the results should localize within the bounds. One might be tempted to loosen the bounds and allow the data to lead to the proper area of parameter space. However, the data do not always have the required leverage to make this a successful approach. For example, if the equation of state rapidly oscillated between -10 and $+10$, this could not be detected in the distance measurements (or such an oscillation in ionization fraction, even to unphysical negative values, might not be seen in cosmic microwave background polarization measurements), but one has spent a lot of effort calculating over an enlarged range. Furthermore, when dealing with systematics, unknown by definition, or projected future measurements, if one does not bound the amplitudes then no real information can be obtained from the results. Thus, one has to balance reasonable, physical bounds and the computational efficiency with the desire not to restrict the input. We take W_-, W_+ to be defined with this in mind. The effects on the principal components of increasing the envelope are simply given by scaling W_-, W_+ in the formulas derived.

The question then becomes how to best incorporate these bounds in "configuration" (e.g. redshift) space into the coefficients of the principal components (PC) in mode space. For example, to generate realizations of state functions that are viable according to the bounds imposed, we must know how to properly sample the PC coefficients.

Several methods can be attempted, but must be assessed for their (computational) efficiency, purity, and completeness. The obvious and least efficient method is simply to try values of the coefficients $\{\alpha_1, \ldots, \alpha_N\}$ and see if the functions $w(z)$ obey the bounds at each redshift. In practice, one must truncate the number of PCs at a finite number N, choose a finite range for each α_i, and (with a number of grid points R sampling the coefficient range) evaluate R^N functions to test whether they lie within the bounds. For a grid of 20 points and 10 PCs, this requires $20^{10} \approx 10^{13}$ evaluations. We call this the scanning strategy. It is pure and complete, but is not efficient.

A second approach is to ask that each PC contribution to the state function obey the bounds individually. This mode-by-mode strategy has been implemented in [4,5,8], for example. Projecting a given PC against the state function yields the coefficient

$$\alpha_i = \mathcal{N} \int dz e_i(z)[w(z) - w_b(z)], \tag{3}$$

where $\mathcal{N} = 1/\int dz e_i^2(z)$ is the normalization factor. Incorporating the bounds on the state function and breaking the integration region into those redshifts where $e_i(z)$ is positive and those where it is negative, one obtains the bounds

$$\alpha_i^- \le \alpha_i \le \alpha_i^+, \tag{4}$$

where

$$\alpha_i^{\pm} = (\mathcal{N}/2)\int dz\{[W_+(z) + W_-(z)]e_i(z) \pm [W_+(z) - W_-(z)]|e_i(z)|\}. \quad (5)$$

The main problem with this approach is that the modes are treated independently. So if one saturates the bounds on each coefficient, say, then the generated state function may actually lie outside the envelope. Thus, this method is complete but not pure.

One way to incorporate all the mode information is to consider the integral of the square of the state function [5]. Then

$$\int dz[w(z) - w_b(z)]^2 = \mathcal{N}\sum_i \alpha_i^2. \quad (6)$$

Imposing the bounds on the state function then delivers the constraint

$$\sum_i \alpha_i^2 \le (1/\mathcal{N})\int dz \max\{W_+^2(z), W_-^2(z)\}, \quad (7)$$

where the maximum is to be evaluated for each redshift. (This generalizes the expression in [5] to when the envelope is not redshift independent.) We call this the integrated method, and it defines a sphere in the mode coefficient space. This approach guarantees completeness but not purity; i.e. every viable state function can be generated with this set of coefficients, but nonviable ones can be generated as well. By itself, this approach lacks a specific prescription for implementing the selection of α_i's.

An alternate approach is the "global" method, where coefficients are chosen based on the previous coefficient values. For example, choose the coefficient α_1 based on the envelope constraint as if this were the only mode, giving

$$\frac{W_{\mp}(z)}{e_1(z)} \le \alpha_1 \le \frac{W_{\pm}(z)}{e_1(z)}, \quad (8)$$

where the top (bottom) sign holds for $e_1(z) > 0$ (< 0). This is applied for all redshifts under consideration, and the tightest constraints obtained define the range of α_1. Once an α_1 is sampled within the allowed range, one obtains similar bounds on α_2 using, e.g., $\alpha_2 e_2(z) \le W_+(z) - \alpha_1 e_1(z)$, and so on. This global method is simpler, not involving any integrals, although it still involves scanning over choices for the coefficients within their allowed range. However, a value for the coefficient α_i that has been rejected because it lies outside the bounds of Eq. (8), or a similar equation, may actually be valid because another PC counteracts its contribution and pulls the state function back within the envelope. Thus the method is pure; i.e. all generated state functions will be viable, but not complete.

Thus we have generating methods that are complete (mode-by-mode method), pure (global method), pure and complete but inefficient (scanning method), but no obviously optimal method. We address this lack in the next section, and show how all the methods are related.

III. A PURE AND COMPLETE PRESCRIPTION

The physical bounds on the state function are imposed in the redshift space but we need to translate these into PC coefficient space if we want to generate principal component analysis (PCA) realizations of the state function. The problem is that a principal component contributes to the state function over the whole redshift interval considered. Effectively, PCA mixes the values w_i from all redshift bins in the bin basis. Therefore, what the chosen bound corresponds to—a value for the state function at a particular redshift z—is not localized in coefficient parameter space but is described by a linear combination of many modes weighted by their respective coefficients.

A. Hypersurface picture

However, by making use of the properties of linear transformations, and a particularly clear geometric picture, we can implement an exact, fast method for the translation. Consider the envelope on a single w_i. This gives a range, or line segment, along the w_i axis. Combining the envelopes for all redshift bins, i.e. w_i parameters, defines a hypersurface in an N-dimensional space, where N is the number of redshift bins. If the bin bounds do not depend on values w_i in other bins, i.e. each bin is independent (recall the original motivation was to consider state function behaviors without assuming a functional form), then the surface is a hyperrectangle.

The corners of the hyperrectangle are defined by the values $W_{\pm}(z_i)$ of the envelope. These 2^N vertices contain all the information on the boundary between the permitted, i.e. viable, instances of state functions $w(z) - w_b(z)$ and the disallowed or unviable ones. That is, the boundary defines the pure and complete set.

We defined the vertices as sets of w_i coordinates but now let us consider the hypersurface in the PC coefficient space of α_i coordinates. Because the PCA is a (normalized) linear transformation of the redshift bin values, the hypersurface is merely rotated, not distorted or expanded. If we are interested in a subset of M modes, smaller than the maximum number N (there cannot be more modes than the original bins used to define the PCs), then this corresponds simply to a projection of the hypersurface onto the subspace of the M PC coefficients. We illustrate the case of a three-dimensional hyperrectangle projected onto 2 PC coefficients in Fig. 1.

The boundary of the pure and complete set of PC coefficients is defined by connecting the outermost projected vertices, ensuring the boundary remains convex. This follows from the linearity of the transform: the hypersurface is convex and so the projection must then itself be convex. (Note the projected figure is not, in general, rectangular.) The projection can be computed quite quickly

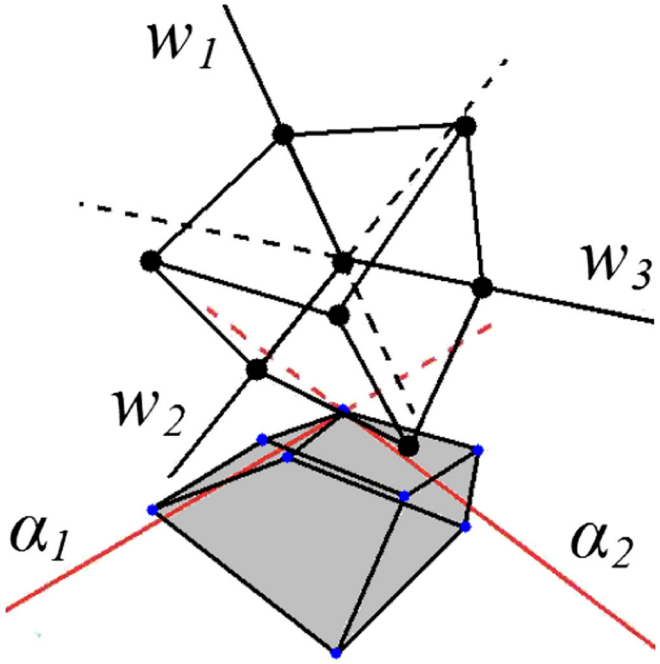

FIG. 1 (color online). A cube in bin space, corresponding to redshift-independent limits on $w(z) - w_b(z)$ in three redshift bins (i.e. the simplest nontrivial case of an N-dimensional hyperrectangle), is projected onto the parameter space of the coefficients of the first two principal components. The small blue dots indicate the projection of the cube vertices. The permitted area in the α_1-α_2 plane is indicated by the light grey shading. Note that it does not form a rectangle.

through the use of matrix algebra (see the Appendix). Thus a pure and complete set of PC coefficients for viable, and only viable, state functions can be generated efficiently.

If we do a complete projection over all N dimensions except one, say α_j, we obtain the absolute minimum and maximum bounds on α_j. These bounds are equivalent to those found with the mode-by-mode method, Eq. (4). Furthermore, since distances are conserved under the linear transformation, the maximum distance in bin space, i.e. the longest diagonal of the hyperrectangle, must also be the maximum distance in PC coefficient space. A (hyper) sphere with this diameter circumscribes the allowed set and corresponds to the sphere of the integrated method, Eq. (7). From the fact that the hypersphere circumscribes the hyperrectangle, it is clear that this method generates a complete, but not pure, set.

The degree of impurity or incompleteness for the methods can be tied to the ratios of areas (or hypervolumes) between the geometric figure defined by the methods and the true hyperrectangle. If the PC coefficients are highly independent of each other (of course the mode vectors e_i themselves are orthogonal), then we expect the mode-by-mode method, where we ignored the effect of α_j on α_i, to be a good approximation, i.e. nearly pure and complete. Taking zero correlation between coefficients defines a rectangle in the α_i-α_j plane, for any α_i, α_j. As the coefficient parameters become more correlated, the mode-by-mode method should become less efficient at finding only the viable state functions, i.e. less pure. Geometrically, the filling factor of the true hyperrectangle projection will decrease.

Figure 2 illustrates this relation between correlation and filling factor. The top panel shows the projection onto the space spanned by the coefficients of PC modes 1 and 17. Since e_1 and e_{17} have their main weights at very different redshifts, the coefficients α_1 and α_{17} are substantially

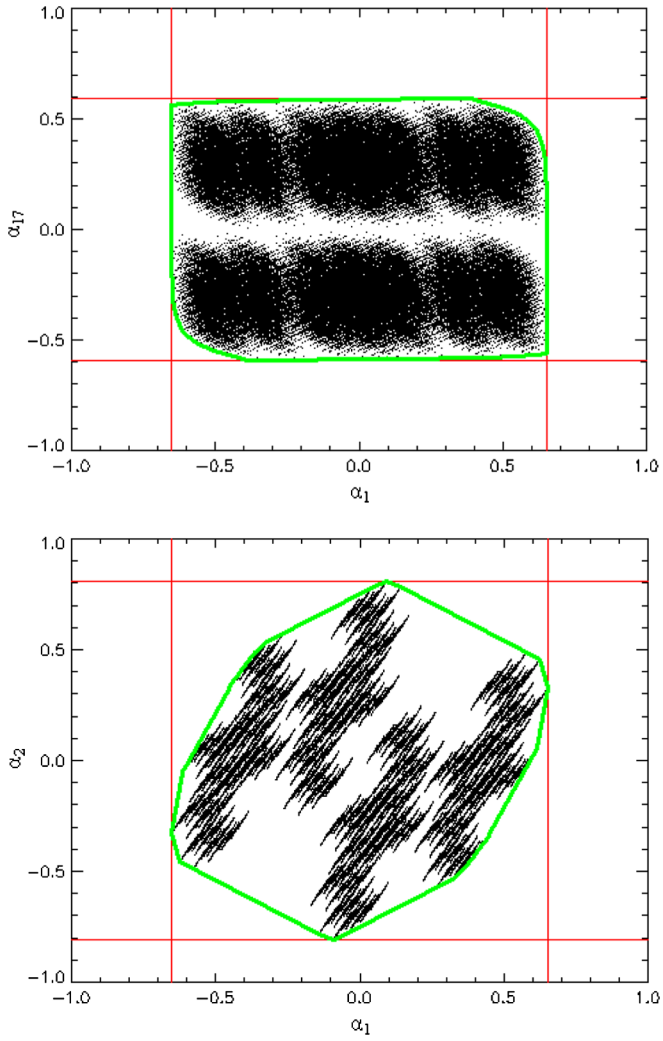

FIG. 2 (color online). Projections onto PCA coefficient planes are shown for the 17 mode case. The light (red) vertical and horizontal lines indicate the mode-by-mode bounds of Eq. (4). The dots give the projection of the 2^{17} vertices of the hyperrectangle, and the thick, green polygon gives the outer boundary, defining the interior region of pure and complete viable state functions. Top panel: The α_1-α_{17} plane in parameter space has low correlation between these modes, so the filling factor of the approximate bounds is high. Bottom panel: The α_1-α_2 plane has strong correlations because the PCs overlap substantially in redshift, so the filling factor is low.

uncorrelated, and indeed the filling factor is high (but not perfect). The bottom panel displays the equivalent projection for modes 1 and 2. Here the overlap of the modes in redshift is greater and so the coefficients are more correlated; the filling factor is noticeably decreased. Therefore the mode-by-mode method is not efficient when considering the dominant modes.

By contrast, the exact hyperrectangle projection method is highly efficient. For 10 modes, say, there are $2^{10} \approx 10^3$ vertices to evaluate (the projection takes negligible computational time using the method in the Appendix). Contrast this with the previous 10^{13} evaluations needed for direct scanning.

If we were to increase the number of redshift bins (i.e. bin modes, holding the redshift range constant), this allows for more and more PC modes. However, since most of these additional modes would be less and less correlated with a given mode, we effectively have a convergence in the behavior of the parameters, i.e. the projected boundary in a given α_i-α_j plane.

In summary, we have presented an efficient, pure, and complete method of obtaining the boundary defining the set of viable state functions. The relation to previous (not simultaneously pure and complete) methods is illustrated in Figs. 3 and 4. The outer rectangle gives the prescription of the mode-by-mode approach; the thick interior polygon shows the exact solution using the projection of the hyperrectangle; and the light shaded interior nonrectangle illustrates the global method, representing a cut through the hyperrectangle at $\alpha_{i>2} = 0$. Since the exact solution can be generated efficiently, there is no need to use the over (global) or under (mode-by-mode) approximation.

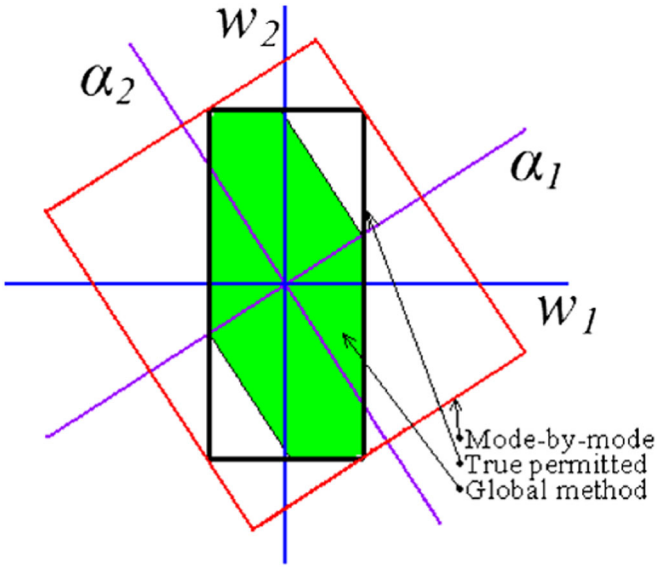

FIG. 3 (color online). Three different approaches to obtaining the principal component coefficients for a constrained state function are illustrated, here for the first and second coefficients and the simplest case with only two modes. The true viable region is the thick black rectangle in w_1-w_2. The shaded, green interior polygon shows the pure but incomplete global approximation, while the exterior thin, red rectangle shows the complete but impure mode-by-mode approximation. We do not show the circle circumscribing the outer rectangle that corresponds to the complete but impure integrated approximation.

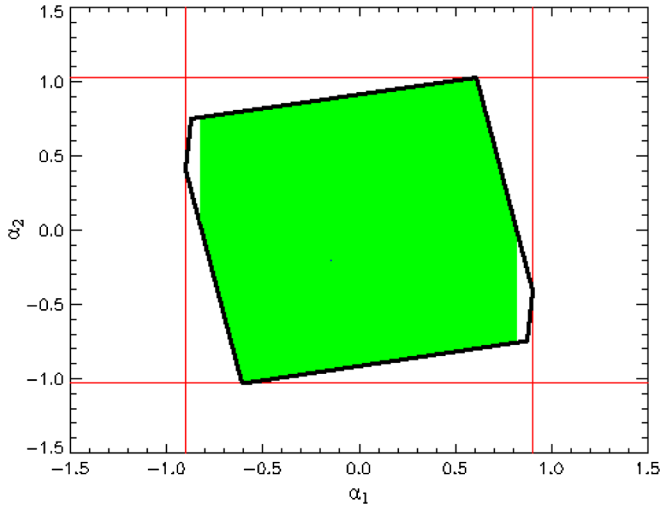

FIG. 4 (color online). Same as Fig. 3 but for three binned w modes projected onto the plane of the first two PC coefficients. Here we suppress the axes. The light (red) vertical and horizontal lines show the mode-by-mode limits; the thick, black polygon defines the exact, pure and complete function space, and the green, shaded region is the global approximation.

While we have solved the problem of obtaining efficiently the constraint on the region of principal component space that is viable given some bounds on the state function, we have to ask whether this is really the best path for analyzing the effect of various state functions. To scan over all viable PCs we would select from the PC coefficients within the allowed region. If the probability of the state function in the bin basis was uniform within the bounds, then because of the linearity of the principal component transformation the interior volume in PC coefficient space can also be uniformly sampled. However, in general, we would have some correlation

$$\langle \alpha_i \alpha_j \rangle = e_{ip} e_{jq} \langle w_p w_q \rangle, \tag{9}$$

where angle brackets denote the ensemble average and p, q are redshift bin indices (implicitly summed) while i, j are component mode indices.

Writing this in matrix notation,

$$A = EWE^T, \tag{10}$$

where W is the correlation of the state function (e.g. equation of state values in redshift bins) and A is the correlation that then must be imposed on the selection of PC coefficients. Note that when the bounds on the state function are redshift dependent—as when some data con-

straint knowledge is incorporated—then even a diagonal W does not lead to a diagonal A.

B. Restricting modes

If we keep only M modes in PC space, then, because the α_i axes are not, in general, aligned with the bin basis w_i axes, the PCs will still span the redshift range but will not be able to describe the full range of $w(z)$ behaviors within the true bounds. That is, we diminish the completeness if we restrict the number of PC modes. Note this can be treated in the hyperrectangle picture as slices through the N rectangle at fixed values of the neglected $N - M$ parameters (see the Appendix for more details). Figure 5 shows an example of the diminished state function space accessed when limiting to four modes (out of 17). Moreover, the impurity of the mode-by-mode method becomes more severe, with Fig. 6 showing that using less than the full number of modes can yield up to 70% of the generated forms of the state function being spurious, i.e. ones that invalidly exceed the bounds, under the restriction to the first M modes.

In the end, then, because of the coefficient correlations and the completeness issues, little advantage accrues in fact to the use of PCA for the scanning over functional forms. It is more efficient (and innately pure and complete) simply to carry out the analysis in the original state function space where the constraints originated. A standard redshift bin basis allows the freedom needed to model the form of the state function, and the constraints can be imposed naturally without complicating the generation of realizations. In the next sections we demonstrate the real world application of the bin basis state functions to problems involving calculating the effects on cosmology results when confronted with unknown systematics functions.

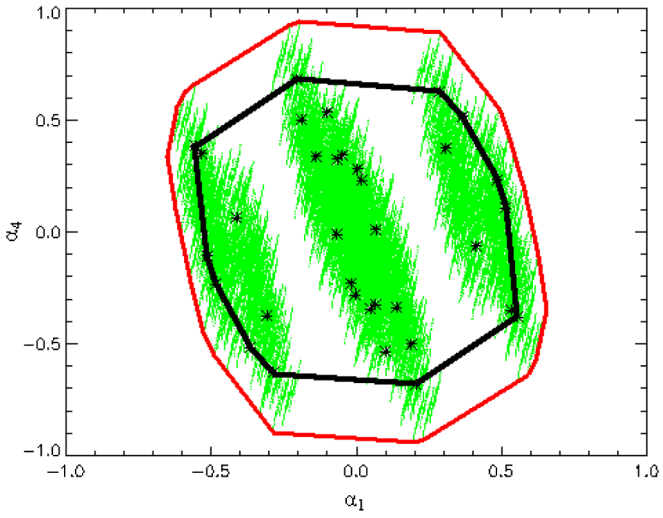

FIG. 5 (color online). Restricting the number of PC modes kept in the analysis will lose completeness in the state function forms allowed. The light (green) dots show the projection of the full set of hyperrectangle corners, with the light (red) outer polygon giving the pure and complete bounds in α_1-α_4 space. The black dots and black polygon show the case when only the first four modes are kept. The region in between the polygons represents viable but lost state functions.

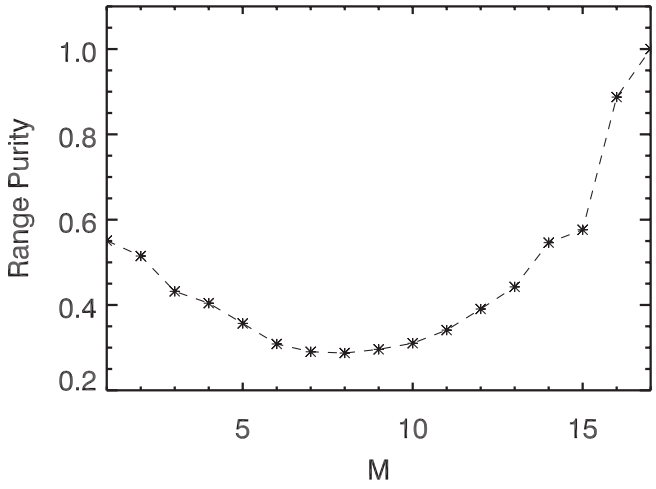

FIG. 6. When not all PC modes are kept, then the purity of the mode-by-mode method decreases. The curve shows the range purity—the product of the bounds on each PC coefficient for the exact method when only M modes are retained vs when all modes are. This is also equivalent to the ratio of the M mode range area to the mode-by-mode method's area.

IV. SYSTEMATICS: SUPERNOVA POPULATION DRIFT

The use of constrained functions, and their impact on parameter estimation or the science results, enters into myriad areas of cosmology. This is a particularly important issue for systematic uncertainties, where we do not know the form of the residual error function. We therefore consider the example of the population fraction of a certain type of source as a key element of the cosmology calculation and take as the state function the uncertainty in our knowledge of it. By definition the function is constrained to take values in the range [0, 1]. If the source is a standardized distance indicator such as type Ia supernovae (SNe) and we posit that the populations represent subclasses with slightly different intrinsic magnitudes, then any variation with redshift in the population fractions will appear as magnitude evolution and, if unrecognized, bias the cosmological parameter estimation. This is known as population drift (for a theoretical discussion and observational limits see [11–16]).

In [9], the effects of population drift, as a bias or increased dispersion (if adding fit parameters), on cosmology were investigated for a class of state functions depending on redshfit as a power law (also see [17]). Here we can analyze *every* form of population drift and investigate which is the most dangerous. In addition, we refine our quantification of the cosmology bias and explore in what

redshift ranges the population drift systematic is most biasing.

Population drift as a systematic relies on two elements: an actual difference in intrinsic magnitudes between the subclasses and a redshift dependence in the difference. A mere constant difference is absorbed into the absolute magnitude nuisance parameter $\mathcal{M}$. For simplicity, we illustrate the basic results for a two population model, where the SNe have a fraction $f_1(z)$ with intrinsic magnitude M_1 and a fraction $f_2(z)$ with intrinsic magnitude M_2. We can consider f_1 as representing all the populations we recognize and $f_2 = 1 - f_1$ as an aggregate of those unrecognized. Then the unrecognized systematics appears as a magnitude evolution

$$\Delta m(z) = \Delta M[f(z) - f(0)], \tag{11}$$

where $\Delta M = M_2 - M_1$ and $f = f_2$ is now our state function. The constraint on the state function, by definition of the population fraction, is $f \in [0, 1]$.

Propagating this systematic through to the cosmology parameters is straightforward. For a parameter set $\vec{p} = \{p_i\}$, the bias is (see, e.g., [18])

$$\delta\vec{p} = (U^T C^{-1} U)^{-1} U^T C^{-1} \Delta O, \tag{12}$$

where O is the observable, $U = \partial O/\partial\vec{p}$, C is the error covariance matrix for the observables, and ΔO is a systematic offset in observable O. The term in parentheses is simply the Fisher matrix, and so its inverse is the parameter covariance matrix. In the case we are currently considering, the observables O are SN magnitudes at various redshifts and ΔO is the magnitude offset of Eq. (11). For a diagonal error covariance matrix the equation takes a simpler form,

$$\delta p_i = \Delta M (F^{-1})_{ij} \sum_{k=1}^{N} f(z_k) \frac{1}{\sigma^2(m_k)} \frac{\partial m_k}{\partial p_j}. \tag{13}$$

Here F is the Fisher matrix, say 4×4 with respect to $\mathcal{M}$, Ω_m, w_0, and w_a, where Ω_m is the present matter density in units of the critical density. There are N data points, each with an associated redshift z_k.

We can now explore the effect of any form for $f(z)$, subject only to the constraint $0 \le f(z) \le 1$. We do not need to assume a functional form for f; rather, we want to allow it complete freedom under constraint. As we saw in the previous section, no real advantage accrues to a principal component analysis—all the information exists and is more accessible using a redshift bin basis. In fact, when keeping only a more limited number of modes, PCA loses information and the bin basis allows for greater efficiency in scanning the allowed state function parameter space.

Before we calculate the bias we examine in more detail how to assess it quantitatively. The bias δp_i itself is only informative together with the cosmological parameter uncertainties. If the estimated uncertainty on the parameters is large, then the relative effect of a particular bias is lower, meaning that the (mis)estimated model is still within some acceptable confidence level contour. For each parameter p_i, Ref. [9] employed the risk statistic [19]

$$\text{risk}\,(p_i) = \sqrt{\sigma_{p_i}^2 + \delta p_i^2} \tag{14}$$

as a measure of the influence of the bias. However, the overall cosmology is biased by the vector $\delta\vec{p}$. One could imagine that each parameter bias relative to the dispersion is small, but in a direction such that $\delta\vec{p}$ is oriented along the thin part (minor axis) of the confidence level contour; then a small shift could actually be a large bias relative to the contour, i.e. in terms of the $\Delta\chi^2$. Following [20] (cf. [21]), therefore, we use as our bias statistic

$$\Delta\chi^2 = \boldsymbol{\delta p}\mathbf{F}^{(r)}\boldsymbol{\delta p}^T, \tag{15}$$

where $\boldsymbol{\delta p}$ is the vector of parameter biases we consider and $\mathbf{F}^{(r)}$ is the reduced Fisher matrix, marginalized over all parameters except those in whose biases we are interested. For example, if we consider biases in the w_0-w_a contour, then $\mathbf{F}^{(r)}$ is the inverse of the 2×2 submatrix of the covariance matrix containing w_0 and w_a. In the case of a single parameter, $\Delta\chi^2 = (\delta p/\sigma_p)^2$ and risk $= \sigma_p\sqrt{1 + \Delta\chi^2}$.

We can now scan over all possible population drifts $f(z) - f(0)$ and evaluate the bias effects on the cosmological parameters. We write f in the redshift bin basis, initially with 17 bins uniform in the range $z = 0$–1.7. For the Fisher matrix we take simulated data based on the SNAP SN redshift and error distribution [22], plus a Planck-inspired constraint on the reduced distance to CMB last scattering of 0.2%. The fiducial cosmology is ΛCDM with matter density $\Omega_m = 0.28$.

Table I describes the population evolution functions computed to deliver the maximum bias in $\Delta\chi^2$. The results have a very simple form: a single or double sharp transition in redshift. This can be understood through analyzing Eq. (13). The bias is a linear transformation of f; hence

TABLE I. For each set of parameters we consider the form of population evolution that maximizes the cosmology bias in terms of $\Delta\chi^2$. The z_{trans} column gives the redshift of the maximizing step function in f, delivering a maximum bias $\Delta\chi^2$ scaled to the case where $\Delta M = 0.01$, which is shown in the next column. Note $\Delta\chi^2$ will scale as ΔM^2. The last column shows the value of ΔM that will shift the derived cosmology by 1σ from the true cosmology.

Parameters	z_{trans}	$\max\Delta\chi^2_{\Delta M=0.01}$	$\Delta M(1\sigma)$
Ω_m	0.7	0.92	0.010
w_0	0.2, 1.0	1.35	0.0086
w_a	0.1, 1.0	1.35	0.0086
w_0, w_a	0.1, 1.0	1.36	0.013
Ω_m, w_0, w_a	0.1, 0.9	1.39	0.016

for a maximum bias, f is driven to the extreme value that complements the sign of the term $\beta_i \equiv (F^{-1})_{ij}\partial m_k/\partial p_j$, for each z_k. To maximize δp_i, when $\beta_i > 0$ then f should be 1, while when $\beta_i < 0$ then f should be 0. This will give coherent addition of the terms in the sum and so deliver the largest δp_i. Thus f should simply be a series of top hats over those redshifts where $\beta_i(z_k)$ is positive. For the parameter Ω_m, β_{Ω_m} crosses once through 0, so $\delta\Omega_m$ is maximized by a population function that has a single transition, at $z \approx 0.7$. Thus the most potent evolution function f—the one having the strongest consequence for cosmology estimation—has a step appearing at $z = 0.7$ and extending to the maximum redshift. For w_0 or w_a, the respective β's cross twice through 0, so f forms a top hat extending from $z \approx 0.2$ (respectively 0.1) to $z \approx 1.0$.

This has a number of crucial implications. First, since the state function with the maximal effect arises from a sharp transition, we see that it was prescient to use the bin basis for the population function. Had we transformed to principal component space, or some smooth orthogonal basis such as the Chebyshev polynomials considered by [9,10], then we would have had difficulty approximating the true solution with a finite number of modes. Second, the sensitivity to population evolution at specific redshifts guides the survey design to obtain especially detailed measurements at these redshifts. The results indicate that as observations make the transition from local ($z < 0.1$) SNe to low redshift ($z \gtrsim 0.2$) SNe, they must comprehensively collect and study the SN properties so as to ensure a firm like-to-like comparison and not allow for unrecognized populations. Similarly, the transition from $z < 1$ to $z > 1$ SNe is key, so a transition from ground-based observing to space-based observing necessitated at $z > 1$ could be problematic. A homogeneous survey extending across this transition would have far better control over the systematic uncertainty.

These results hold as well when simultaneously considering bias in multiple parameters in the $\Delta\chi^2$ formalism. The population f enters Eq. (15) quadratically and so the bias is still maximized by the extreme values of f, i.e. top hats in redshift. The transition locations do not shift appreciably when considering bias in the two parameter space of w_0-w_a nor the three parameters Ω_m, w_0, w_a simultaneously. Furthermore, the transition locations are robust to changing the step functions to more gradual slopes.

The last column of Table I shows the magnitude of ΔM that, in the worst case of population evolution, causes a 1σ misestimation of the cosmology. This is where the scaling of the state function bounds enters: the shape, i.e. redshift dependence of the population function, is unaffected by amplitude of the bounds, but the absolute level is determined by the bounds. If we consider values twice as large for ΔM (or if we were to unphysically allow f to range from 0 to 2), then $\Delta\chi^2$ just scales with ΔM^2. If we want to be sure that population drift cannot cause a $>1\sigma$ shift in the equation of state parameters, we need to be able to recognize SN subclasses differing by 0.0086 mag or more.

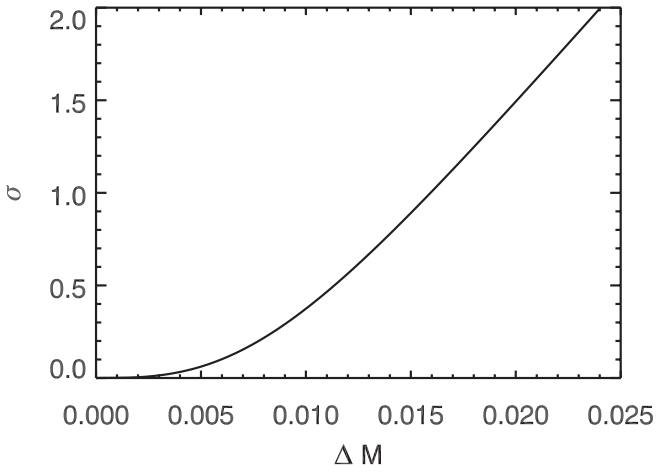

FIG. 7. For the maximally biasing population drift the cosmological parameter set $\{\Omega_m, w_o, w_a\}$ is biased by 1σ for a population magnitude difference $\Delta M = 0.016$ mag. The curve shows by how many σ the best fit cosmology is biased as a function of ΔM.

Figure 7 shows the relation between the maximum number of standard deviations σ by which the cosmology is distorted, as a function of difference in absolute magnitudes ΔM between the populations, for the full set of cosmological parameters. While $\Delta\chi^2$ scales as ΔM^2, the number of σ this bias corresponds to only scales as ΔM in the one parameter case. We see that for three parameters the σ remains nearly linear for large ΔM but does not improve as rapidly for $\Delta M < 0.015$.

Beyond the maximum $\Delta\chi^2$, we can investigate other properties of the biasing. For example, we can explore further the direction of the systematic shift caused in the cosmology parameters, the relation of the forms of the population drift, i.e. the number of steps or oscillations, to the bias, and the overall statistics of the biasing.

We begin with the effect on the equation of state estimation caused by the systematic error. Figure 8 shows the specific form of bias induced in the equation of state by the 10 worst-case population drifts. The worst biases all distort the cosmology in the same way: making a cosmological constant look like a rapidly varying equation of state. Indeed, this is characteristic not just of population drift but of any sharp transition in the SN magnitudes, such as from patching together two redshift samples with an unrecognized offset (local to low redshift samples, or ground-based to space-based). This points out the need for tight cross-calibration, and ideally a continuous, homogeneous data set, as well as the need for caution in interpreting an apparent behavior of the equation of state crossing $w = -1$: exactly what is expected from such a systematic.

The influence of the forms of the population evolution function on the bias generated in the cosmology parame-

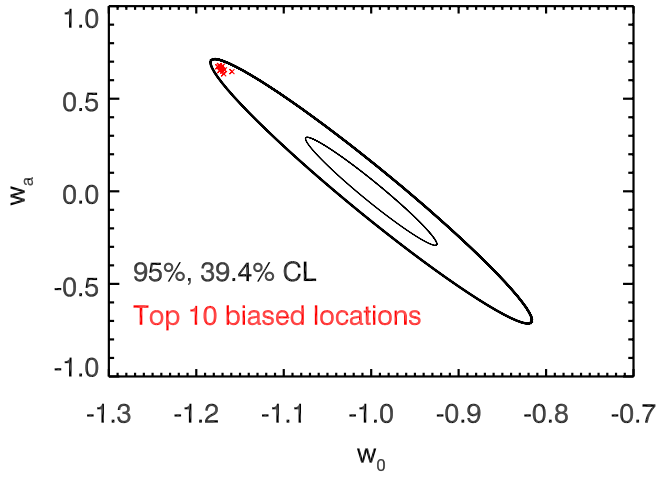

FIG. 8 (color online). The biases induced for $\Delta M = 0.02$ by the worst population evolution functions—those that induce the 10 largest $\Delta\chi^2$—are plotted in the w_0-w_a plane as x's. Note how they congregate at the extreme end of the major axis of the confidence contour. The inner ellipse indicates the 39% confidence level contour [so $\sigma(w_0)$, $\sigma(w_a)$ are given by direct projection to the respective axis], while the outer ellipse shows the 95% C.L. joint likelihood contour.

ters can be investigated through looking at the statistics of the $\Delta\chi^2$ distribution. For example, while the maximum bias is generated from a population function with one or two steps at sensitive redshifts, we expect a large number of transitions to have relatively little effect since such an oscillatory behavior does not resemble the effect of a cosmological parameter. The sum of the terms in Eq. (13) effectively cancels out. Thus certain types of systematics are fairly benign, such as quasiperiodic k-correction errors [23,24]. Figure 9 shows the range of

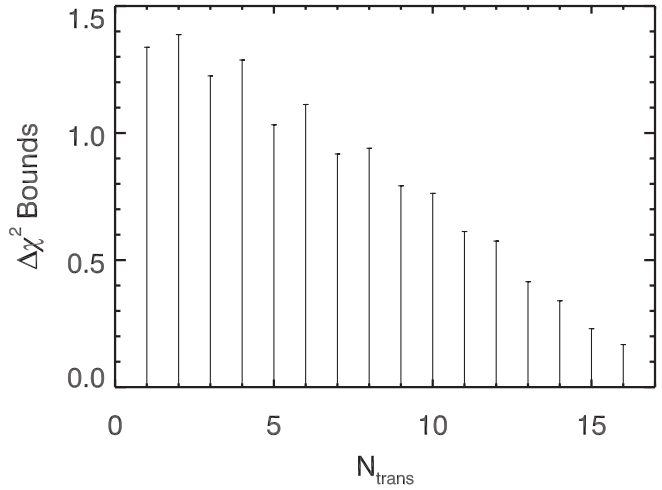

FIG. 9. The range of possible biases $\Delta\chi^2$ in the cosmology likelihood contour for Ω_m-w_0-w_a is plotted vs the number of transitions (changes in value between the 17 redshift bins) in the population evolution.

$\Delta\chi^2$ generated as a function of the number of transitions in f between redshift bins. As expected, as the number of transitions gets large, the bias decreases. Similarly, when the step amplitude is small, then the bias is negligible so the $\Delta\chi^2$ distribution ranges between 0 and the maximum for each number of transitions.

The location in redshift of the features in the population function also is important. As we saw in Table I, $z \approx 0.1$ and $z \approx 1$ were key regions for sensitivity to bias. In Fig. 10 we plot the redshift locations giving not just maximum bias, but greater than a certain percentage of maximum bias (still keeping full steps, i.e. $f = 0$ or 1). We see that, down to 50% of the maximum possible bias, the culprit is still population evolution around these sensitive

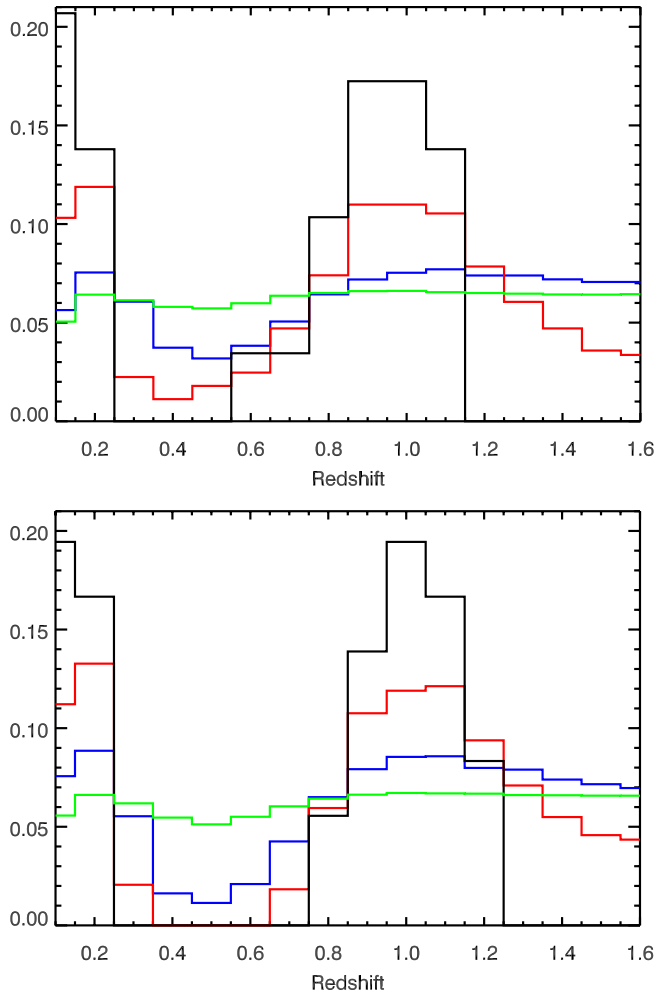

FIG. 10 (color online). The histograms show the redshift locations of the most sensitive steps in the population function f for various cuts in $\Delta\chi^2$. In order from highest to lowest peak, the cuts are 90%, 75%, 50%, 25% of the maximum possible $\Delta\chi^2$. The top panel considers the $\Delta\chi^2$ bias for the cosmology likelihood contour in the Ω_m-w_0-w_a space while the bottom panel is for the w_0-w_a space. Note that the most sensitive redshifts are robust to lower levels of bias, down to 50% of maximum, and to the parameter space considered.

redshifts. This suggests that surveys designed to recognize population subclasses through especially comprehensive measurements around these redshifts can remove the top half of possible cosmology bias, improving the systematics by a factor of 2.

If we consider every possible form of the population function, randomly scanning over the number of steps and locations of transitions, then most of these will have little effect on the cosmology. The mean bias, or $\langle \Delta\chi^2 \rangle$, will therefore be small. For example, the mean is only 0.08 for the w_0-w_a contour. This is simply due to combinatorics: there are many more ways of having, say, eight steps over 17 bins than one step—some 24 000 times more possibilities—and multistep functions will have little impact on the cosmology. Furthermore the random location of the steps will also dilute the mean bias. However, random population evolution is not the issue; for survey design we have to consider the worst-case scenario, i.e. which systematics can give the most egregious misestimation of the cosmology results, and how to control this. The results indicate that experiments should be guided by requirements to recognize subtypes with magnitude differences down to $\sim$0.01 mag (Fig. 7), and with particularly comprehensive measurements around $z \approx 0.1$ and $z \approx 1$ (Fig. 10).

V. SYSTEMATICS: DUST CORRECTION AND CALIBRATION

The analysis of the constrained state function in terms of population drift was particularly straightforward because of the linear relation between the function $f(z)$ and the observable $m(z)$. To illustrate a more complicated application we consider the systematic uncertainty due to the dust extinction correction in supernova distances. This is currently one of the dominant systematics [25–29] and uses measurements in multiple wavelength bands, or filters, to correct for the dust effects. However, if the different filters have some uncertainty in their calibrations then this propagates through to the relative fluxes or colors and then to the dust correction [30]. We use a simple, two band version of this as an illustration of a nonlinear, constrained systematic.

We take the systematic to arise from zero-point calibration errors in each filter, and the constraint can arise from subsidiary measurements such as on standard stars or instrumental calibration (see, e.g., [31]) that limit the zero-point offsets to lie within $\Delta Z \in [Z_-, Z_+]$. Again, it is the relative zero-point differences, or colors, that cause bias; uniform offsets do not affect cosmology. Because the flux from sources at different redshifts peaks in different wavelength bands, the zero-point errors will induce a redshift-dependent error in the magnitude and hence a bias in the cosmology parameter estimation. In addition, because the use of multiple bands to define the dust correction leads to an interdependence of SNe at different redshifts, a correlated error matrix enters [30].

In the two band toy model for dust correction, the corrected magnitude $\tilde{m}$ is related to the magnitudes measured in two neighboring bands by

$$\tilde{m}_i = (1 + R)m_i - Rm_{i+1}, \tag{16}$$

where R is the extinction ratio. We use as the two bands the rest-frame B and V bands for each supernova, take $R = 2.1$ (somewhat emphasizing the effect), and consider only calibration zero-point error contributions to the dust correction, not any intrinsic SN color variation. This simple model is sufficient to illustrate the effects of a nondiagonal error covariance matrix

$$C = BEB^T, \tag{17}$$

$$B = (1 + R)\delta_{ij} - R\delta_{i,j-1}, \tag{18}$$

where E is the precorrection, possibly diagonal, error covariance matrix.

The Fisher matrix is formed using the nondiagonal error covariance matrix C, and we then calculate the parameter bias due to zero-point offsets ΔZ_k in the magnitudes by means of Eq. (12). We consider 8 filters logarithmically spaced in wavelength, with centers at $\lambda_0(1 + a_\star)^{k-1}$, for $k = 1$–8, taking $\lambda_0 = 4400$ Å and $a_\star = 0.15$, so the maximum redshift corresponds to 1.66 [32]. Our state function is ΔZ, which can be both positive and negative within the bounds, and we scan over all possible forms within the bounds and analyze the cosmology bias.

Table II presents the results in the same format as the previous case in Table I. However here the steps are in band zero points not population fractions and the locations are listed in terms of the filter numbers. The important quantity is $\Delta Z_{\rm rel}$ between filters (recall that an overall zero-point error has no cosmology effect), and needs to be constrained to the $\sim$0.01 level. The furthest red filters, used for the highest redshift SNe, are among the most sensitive to bias and should be tightly calibrated with instrumental and standard star measurements.

TABLE II. For each set of parameters we consider the form of filter zero-point errors that maximize the bias in terms of $\Delta\chi^2$. The transitions column gives the filter transitions of the maximizing function in ΔZ, delivering a maximum bias $\Delta\chi^2$ scaled to the case where the zero-point calibration is bounded by $|\Delta Z| = 0.01$, which is shown in the next column. The last column shows the value of $\Delta Z_{\rm rel}$ *between* two filters that will shift the derived cosmology by 1σ from the true cosmology.

Parameters	Transitions	$\max\Delta\chi^2_{\Delta Z=0.01}$	$\Delta Z_{\rm rel}(1\sigma)$
Ω_m	2–3, 7–8	4.07	0.0098
w_0	1–2, 4–5, 7–8	2.79	0.012
w_a	1–2, 4–5, 7–8	2.99	0.012
w_0, w_a	3–4, 7–8	4.12	0.015
Ω_m, w_0, w_a	3–4, 7–8	4.55	0.018

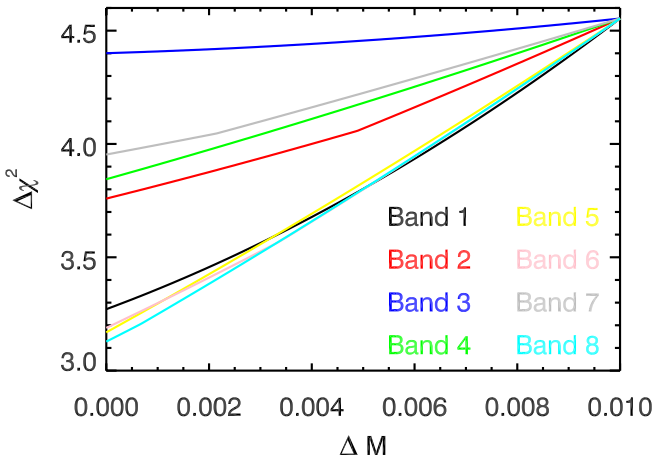

FIG. 11 (color online). The maximum $\Delta\chi^2$ bias is plotted as a function of the bound on individual filter band zero-point offsets. The greatest improvement in systematics control comes from improving the calibration uncertainty ΔZ for bands 1, 5, 6, 8, which correspond to the most cosmologically sensitive redshift leverages, near $z \approx 0$, 1, 1.7.

As in the previous case in Sec. IV, the shape, i.e. wavelength dependence of the zero-point calibration, is unaffected by amplitude of the bounds on the calibration state function, but the absolute level is determined by the bounds. If we consider values twice as large for ΔZ, then $\Delta\chi^2$ just scales with ΔZ^2.

Any filter zero-point step affects SNe in some redshift range, and hence the overall cosmology. Thus an improvement in the knowledge of a filter offset ΔZ_k reduces the maximum $\Delta\chi^2$ bias. Figure 11 shows the effect of more tightly calibrating a given filter.[1] We see the greatest improvement for the end bands—which are used for the lowest-redshift, anchoring SNe and the highest-redshift, lever-arm SNe—and the middle bands, which are used near the sensitive $z \approx 1$ region. Thus survey design that provides particularly comprehensive calibration for these bands will see a large payoff in systematics control.

VI. CONCLUSIONS

Modeling unknown functions in cosmology is pervasive, whether these are functions that carry the physics we are directly interested in, such as the dark energy equation of state history, or functions describing subsidiary effects that we wish to subtract out, such as intermediate astrophysics or modeling of uncertainties. If the functional form is assumed, then this becomes parameter fitting or "self-calibration," but it is interesting and important to investigate the results when any viable function is allowed. The viability is subject only to some constraints placed on the bounds of the function through theoretical or measurement input.

We investigated two main issues for cosmological analysis in the presence of unknown but constrained functions. First, we demonstrated a computationally efficient, pure and complete method for determining the viable space of principal component coefficients, with a simple geometric picture in terms of a hyperrectangle in the N-dimensional basis space. This improves on the efficiency of the previous mode-by-mode method by a factor of 3, while guaranteeing purity, i.e. validity of the selected functions. Conversely, compared to the also pure and complete direct scanning method, the projected hyperrectangle method gains in efficiency by factors of 10^{10} or greater.

For many astrophysical problems the orthogonal bin basis (in redshift or wavelength) is well suited. We evaluated two "real world" systematics issues with this method, one in redshift and one in wavelength. The first dealt with unrecognized population evolution in a subclass of standard candles. Rather than assuming a form of evolution, we analyzed the effects of all possible functional forms lying within some bounds. The results provide quantitative guidance to controlling the worst cosmology biases arising from the systematic uncertainties. In particular, we find that the regions $z \approx 0.1$ and $z \approx 1.0$ can benefit most from comprehensive observations to limit unrecognized subclasses (at the $\sim$0.01 mag level); surveys homogeneous over these redshift regions have improved control over cosmology misestimation.

The second application concerned dust extinction corrections for type Ia supernovae, where measurements in multiple wavelength bands can fit for dust but also correlate supernovae at different redshifts. We analyzed the case where systematic uncertainties existed in the filter calibrations, bounded by instrumental or standard star observations, and propagated all possible functional forms into cosmology biases. Again we found which specific forms were most damaging and that measurements designed to control such errors could remove the worst biases. In particular, those bands used for the lowest and highest supernovae, and ones relevant around $z \approx 1.0$, should be most comprehensively calibrated (to the $\sim$0.01 mag level relatively) for a more robust survey.

ACKNOWLEDGMENTS

We are grateful for useful discussions with Marina Cortês, Alex Kim, Saul Perlmutter, and especially Roland de Putter. J. S. acknowledges support from the OTICON Fund and Dark Cosmology Centre, and thanks the Berkeley Center for Cosmological Physics and the Berkeley Lab for hospitality during his stay. This work has been supported in part by the Director, Office of Science, Office of High Energy Physics, of the U. S.

[1]We have also carried out PCA on the filter model Fisher matrix but find little useful information from the modes. The wavelength-band bin basis is better suited to actual design than saying, e.g., calibrate the combination of 0.4 times the first filter and -0.2 times the second filter, etc.

Department of Energy under Contract No. DE-AC02-05CH11231.

APPENDIX: EFFICIENT PROJECTION AND BOUNDARY DEFINITION

Since the dark energy physics of interest mostly translates into descriptions of the EOS in redshift bin space, our bounds on the state function are given in this space. In this appendix we will detail, through a geometrical understanding, a fast method for analyzing how these bounds in bin space may be carried into bounds on coefficients in principal component space. The bounds on $w(z)$ directly form the space of the permitted sets of these coefficients, but picking a pure and complete set of coefficients in PC space is not so simple.

The value for the EOS, say, at a particular redshift z is not described by just one mode as in the bin space case, but by a linear combination of many modes weighted by their respective coefficients. To scan the whole coefficient space within the bounds given in redshift space requires an impractical amount of computational power, as discussed in Sec. II. We need a more clever method of obtaining the desired results.

For a set of independent state function bounds on $\{w_i\}$, the permitted space in bin space is bounded by a hyperrectangle, or orthotope. The coordinates of the corners are given by any combination $W_1^{\pm}, W_2^{\pm}, \ldots, W_N^{\pm}$, where $W_i^{\pm}$ denotes the maximum and minimum values allowed for bin i, and N is the number of bins. This fixes the 2^N corners. This orthotope structure contains all the needed information on the boundary of the allowed space no matter the basis.

Let us first address how to determine the viable region for any set of principal component coefficients, $\alpha_1, \ldots, \alpha_m$. The permitted space is simply the projection of the orthotope onto the subspace spanned by these components. The nodes of the boundary in PC space are found by projecting the vectors going from the origin to the corners of the orthotope. Denoting these (N-dimensional) vectors as $\mathbf{c_i}$ and the projected (m-dimensional) node vectors in the $\mathbf{S} = [e_1, \ldots, e_m]$ PC space as $\mathbf{p_i} = (p_{i1}, \ldots, p_{im})$, where $p_{i1}, \ldots, p_{im}$ are the coordinates of $\mathbf{p_i}$ with respect to the axes $\alpha_1, \ldots, \alpha_m$, we find

$$\mathbf{p}_\mathbf{i} = (\mathbf{S}^T\mathbf{S})^{-1}\mathbf{S}^T\mathbf{c_i}. \tag{A1}$$

Consider now the case where we keep only a subset of PC modes, i.e. we do not marginalize over the other modes but fix their coefficients, e.g. to 0. Information is lost by not using the complete basis in the expansion, but sometimes data or practicalities do not enable us to know or measure all modes. Therefore, we must sometimes sample with only a subset M of modes. The new permitted space of PC coefficients is the intersection of the M-dimensional space with the original N-dimensional space. This subspace is completely defined by the boundary points, found by looking at the intersections between the M-dimensional space of interest and the N-dimensional bounded bin space (cf. the black dots in Fig. 5). However, the allowed space is generally not an M rectangle; for example, a plane cutting through a cube can have a boundary with six corners unless it is specially oriented. This has the consequence that there is no M-dimensional basis that will generally be pure and complete (i.e. there are no orthogonal axes spanning the space). Only the original bin basis in N dimensions can provide a pure and complete description of the valid state functions.

To describe the actual procedure for evaluating the allowed region in PC space we rephrase the issue more mathematically. The determination of the coefficient bounds is solved by considering the intersection of the subspace $\mathbf{C_a}$, spanned by the principal components keeping the selected number of coefficients constant, with the orthotope. In the three-dimensional case, with a two-dimensional subspace, the boundaries are of $3 - 2$ dimensions, i.e. lines, having parametric form $\mathbf{I}_a + (\mathbf{I}_b - \mathbf{I}_a)t$, and the plane is parametrized by $\mathbf{P}_0 + (\mathbf{P}_1 - \mathbf{P}_0)u + (\mathbf{P}_2 - \mathbf{P}_0)\upsilon$, where t, u, υ are real numbers, and $\mathbf{I}_i$ and $\mathbf{P}_j$ are points on the line and in the plane, respectively. Setting $\mathbf{D} = [\mathbf{I}_a - \mathbf{P}_0]$, $\mathbf{A} = [\mathbf{I}_a - \mathbf{I}_b, \mathbf{P}_1 - \mathbf{P}_0, \mathbf{P}_2 - \mathbf{P}_0]$, and $\mathbf{L} = [t, u, \upsilon]$, we find

$$\mathbf{D}^{-1}\mathbf{A} = \mathbf{L}. \tag{A2}$$

In the higher dimensional case the solution has the identical form. Geometrically, $\mathbf{I}$ represents vectors going from the origin to the corners of the orthotope (so $t \in [0, 1]$) and $\mathbf{P}$ are *noncollinear* points in $\mathbf{C_a}$. The matrix manipulations can be computed easily, so solving for the allowed region in PC space is highly efficient and quick.

[1] R. de Putter and E. V. Linder, J. Cosmol. Astropart. Phys. 10 (2008) 042.
[2] D. Huterer and G. Starkman, Phys. Rev. Lett. **90**, 031301 (2003).
[3] D. Huterer and A. Cooray, Phys. Rev. D **71**, 023506 (2005).
[4] R. de Putter and E. V. Linder, Astropart. Phys. **29**, 424 (2008).
[5] M. J. Mortonson, W. Hu, and D. Huterer, Phys. Rev. D **79**, 023004 (2009).
[6] T. D. Kitching and A. Amara, Mon. Not. R. Astron. Soc. **398**, 2134 (2009).

[7] M. J. Mortonson, Phys. Rev. D **80**, 123504 (2009).
[8] M. J. Mortonson and W. Hu, Astrophys. J. **672**, 737 (2008).
[9] E. V. Linder, Phys. Rev. D **79**, 023509 (2009).
[10] T. D. Kitching, A. Amara, F. B. Abdalla, B. Joachimi, and A. Refregier, Mon. Not. R. Astron. Soc. **399**, 2107 (2009).
[11] D. Branch, S. Perlmutter, E. Baron, and P. Nugent, arXiv: astro-ph/0109070.
[12] M. Sullivan *et al.*, Astrophys. J. **648**, 868 (2006).
[13] D. A. Howell, M. Sullivan, A. Conley, and R. G. Carlberg, Astrophys. J. **667**, L37 (2007).
[14] T. J. Bronder *et al.*, Astron. Astrophys. **477**, 717 (2008).
[15] D. A. Howell *et al.*, Astrophys. J. **691**, 661 (2009).
[16] M. Sullivan *et al.*, Astrophys. J. **693**, L76 (2009).
[17] S. Linden, J-M. Virey, and A. Tilquin, Astron. Astrophys. **506**, 1095 (2009).
[18] E. V. Linder, Astropart. Phys. **26**, 102 (2006).
[19] M. G. Kendall, A. Stuart, and J. K. Ord, *Advanced Theory of Statistics* (Oxford University, New York, 1987).
[20] C. Shapiro, Astrophys. J. **696**, 775 (2009).
[21] S. Dodelson, C. Shapiro, and M. White, Phys. Rev. D **73**, 023009 (2006).
[22] A. G. Kim, E. V. Linder, R. Miquel, and N. Mostek, Mon. Not. R. Astron. Soc. **347**, 909 (2004).
[23] T. M. Davis, B. P. Schmidt, and A. G. Kim, Publ. Astron. Soc. Pac. **118**, 205 (2006).
[24] E. Y. Hsiao *et al.*, Astrophys. J. **663**, 1187 (2007).
[25] A. Conley *et al.*, Astrophys. J. **664**, L13 (2007).
[26] M. Kowalski *et al.*, Astrophys. J. **686**, 749 (2008).
[27] M. Hicken *et al.*, Astrophys. J. **700**, 1097 (2009).
[28] S. Nobili *et al.*, Astrophys. J. **700**, 1415 (2009).
[29] J. Nordin, A. Goobar, and J. Jonsson, J. Cosmol. Astropart. Phys. 02 (2008) 008.
[30] A. G. Kim and R. Miquel, Astropart. Phys. **24**, 451 (2006).
[31] C. W. Stubbs *et al.*, ASP Conf. Series **364**, 373 (2007).
[32] G. Aldering *et al.*, arXiv:astro-ph/0405232.